Targeting ferroptosis in rhabdomyosarcoma cells

Jasmin Dächert[1], Vanessa Zimmermann[1], Karoline Habermann[1] and Simone Fulda[1,2,3]

[1]Institute for Experimental Cancer Research in Pediatrics, Goethe-University Frankfurt, Frankfurt, Germany

[2]German Cancer Consortium (DKTK), Partner Site Frankfurt, Frankfurt, Germany

[3]German Cancer Research Center (DKFZ), Heidelberg, Germany

Correspondence to: *Simone Fulda,* ***email:*** *simone.fulda@kgu.de*

Keywords: *ferroptosis; cell death; RMS; redox*

Received: *May 02, 2018* ***Accepted:*** *July 08, 2018* ***Published:***

ABSTRACT

Recent data suggest that rhabdomyosarcoma (RMS) cells might be vulnerable to oxidative stress-induced cell death. Here, we show that RMS are susceptible to cell death induced by Erastin, an inhibitor of the glutamate/cystine antiporter x_c^- that can increase reactive oxygen species (ROS) production via glutathione (GSH) depletion. Prior to cell death, Erastin caused GSH depletion, ROS production and lipid peroxidation. Importantly, pharmacological inhibitors of lipid peroxidation (i.e. Ferrostatin-1, Liproxstatin-1), ROS scavengers (i.e. α-Tocopherol, GSH) and the iron chelator Deferoxamine (DFO) inhibited ROS accumulation, lipid peroxidation and cell death, consistent with ferroptosis. Interestingly, the broad-spectrum protein kinase C (PKC) inhibitor Bisindolylmaleimide I as well as the PKCα- and β-selective inhibitor Gö6976 significantly reduced Erastin-induced cell death. Similarly, genetic knockdown of PKCα significantly protected RMS cells from cell death induced by Erastin. Furthermore, the broad-spectrum Nicotinamide adenine dinucleotide phosphate (NADPH)-oxidase (NOX) inhibitor Diphenyleneiodonium (DPI) and the selective NOX1/4 isoform inhibitor GKT137831 significantly decreased Erastin-stimulated ROS, lipid ROS and cell death. These data provide new insights into the molecular mechanisms of ferroptosis in RMS, contributing to the development of new redox-based treatment strategies.

INTRODUCTION

RMS is the most common soft-tissue sarcoma in children and adolescents. It can be divided into two broad subtypes, namely embryonal RMS (eRMS) and alveolar RMS (aRMS) [1]. Treatment protocols include chemotherapy, irradiation, and surgery [2]. Patients with relapsed or metastatic disease still have a poor prognosis highlighting the high medical need for novel treatment options [3, 4]. One of the hallmarks of cancer is the evasion of programmed cell death, especially apoptosis, favoring cancer progression and resistance [5]. Besides apoptosis, other genetically regulated forms of cell death have been described including ferroptosis [6, 7].

Ferroptosis is characterized as an iron-dependent form of cell death accompanied by accumulation of ROS and lipid peroxidation [8, 9]. It is initiated upon inhibition of GSH peroxidase 4 (GPX4), a GSH-dependent antioxidant enzyme that reduces membrane phospholipid hydroperoxides to suppress ferroptosis [10]. Two classes of ferroptosis-inducing compounds have been described [11]. On the one side, ferroptosis is induced by Erastin that inhibits the membrane-bound cystine-glutamate antiporter x_c^-, leading to depletion of GSH, a necessary cofactor of GPX4 for eliminating lipid peroxides [8, 12]. On the other side, RSL3 triggers ferroptosis by covalent binding to the active site of GPX4, thereby inhibiting its enzymatic function and promoting the accumulation of lethal lipid

peroxides [13, 14]. Besides inhibition of GPX4 and depletion of GSH, ROS-generating enzymes and active labile iron pools can cause increased ROS production [15, 16]. Many ROS-generating enzymes contain iron in their active centers, for example NOX, lipoxygenases, xanthine oxidases and cytochrome P450 enzymes [15, 16].

Recent data suggest that RMS may be vulnerable to oxidative stress [17]. Genomic analysis of primary RMS samples revealed single nucleotide mutations that are characteristic of oxidative stress, indicating increased levels of oxidative damage [17]. Furthermore, RMS xenograft models exhibited sensitivity to several compounds which increased oxidative stress like carfilzomib, auranofin and cerivastatin [17]. Moreover, RMS have been described to display antioxidant defense mechanisms such as increased GSH levels to maintain the redox balance [18], implying that they might be susceptible to GSH depletion. Against this background, we investigated whether Erastin, a known GSH-depleting compound, can be exploited to initiate programmed cell death in RMS.

RESULTS

Erastin induces cell death in several RMS cell lines

Initially, we screened a panel of RMS cell lines for their sensitivity to Erastin, a prototypical stimulus to engage oxidative stress and programmed cell death [8]. Treatment with Erastin for 24 hours triggered cell death in a dose-dependent manner in the majority of RMS cell lines (Figure 1A). While T174 and RH41 RMS cell lines showed a delayed response to Erastin after treatment for 48 hours, Kym-1 remained refractory even to a 48 hour treatment with relatively high concentrations of Erastin (Supplementary Figure 1). Therefore, we investigated whether this differential responsiveness to Erastin is due to differences in xCT levels, the light subunit of x_c^- and a pharmacological target of Erastin [8, 19], since xCT has been described to correlate with Erastin sensitivity [8, 20]. Analysis of xCT mRNA levels showed a large variation in the panel of RMS cell lines (Figure 1B). Plotting of xCT mRNA levels against the percentage of cell death upon treatment with Erastin showed no clear correlation between sensitivity to Erastin and xCT mRNA levels in this limited panel of RMS cell lines (Figure 1C). These results show that Erastin induces cell death in a panel of RMS cell lines irrespective of expression levels of xCT.

Erastin-induced cell death displays characteristic features of ferroptosis

To investigate whether Erastin induces cell death via ferroptosis we tested the effects of several pharmacological inhibitors. Importantly, the ferroptosis inhibitors Liproxstatin-1 (Lip-1) and Ferrostatin-1 (Fer-1), the lipophilic vitamin E derivate α-Tocopherol (α-Toc) and the iron chelator DFO [21, 22] all completely abolished Erastin-induced cell death in RMS cells (Figure 2A, 2B, Supplementary Figure 2A). Also, addition of GSH, a ROS scavenger and cofactor of GPX4 [23], as well as N-acetylcysteine (NAC), a precursor of GSH, completely inhibited cell death (Figure 2B, Supplementary Figure 2B). Similarly, Fer-1 and DFO inhibited cell death induced by RSL3 (Supplementary Figure 2C), a pharmacological GPX4 inhibitor [14] that we used as a positive control for the induction of ferroptosis.

As Erastin inhibits the glutamate/cystine antiporter x_c^- [8], we then determined GSH levels. Consistent with its mode of action, treatment with Erastin for six hours significantly reduced GSH levels in RMS cells (Figure 3A). Importantly, this Erastin-mediated GSH depletion was accompanied by a significant increase in ROS production and lipid peroxidation after 12 hours (Figure 3B, 3C). A kinetic analysis revealed that Erastin triggered cell death in a time-dependent manner starting at 15 to 18 hours (Figure 3D). These findings demonstrate that Erastin causes GSH depletion, ROS production and lipid peroxidation prior to cell death in RMS cells.

Next, we determined the effects of ferroptosis inhibitors, ROS scavengers and DFO on ROS formation and lipid peroxidation. Erastin-induced ROS production was significantly blocked in the presence of Lip-1, Fer-1, DFO, α-Toc or GSH (Figure 4A). Likewise, lipid peroxide formation was significantly decreased by the addition of these inhibitors (Figure 4B).

Together, this set of experiments shows that Erastin-induced cell death displays characteristic features of ferroptosis.

Pharmacological PKC inhibition blocks Erastin-induced cell death and lipid peroxidation

As PKC has recently been implicated in ferroptosis in a model of Parkinson's disease [24], we investigated the involvement of PKC in the control of ferroptosis in RMS cells. To screen for a potential involvement of PKC, we used the broad-range PKC inhibitor Bisindolylmaleimide I (Bim1) that targets different isoforms [25]. Importantly, addition of Bim1 significantly attenuated Erastin-induced cell death in a dose-dependent manner (Figure 5A). Likewise, Erastin-induced ROS production (Figure 5B) and lipid peroxidation (Figure 5C) were significantly reduced in the presence of Bim1.

Next, we analyzed in further detail the involvement of different PKC isoforms. Quantitative real-time PCR analysis revealed that PKCα was more abundantly expressed than PKCδ, ε and β in RMS cells (Supplementary Figure 3). Therefore, we selected the PKCα- and β-selective inhibitor Gö6976 for further experiments [26]. Notably, addition of Gö6976

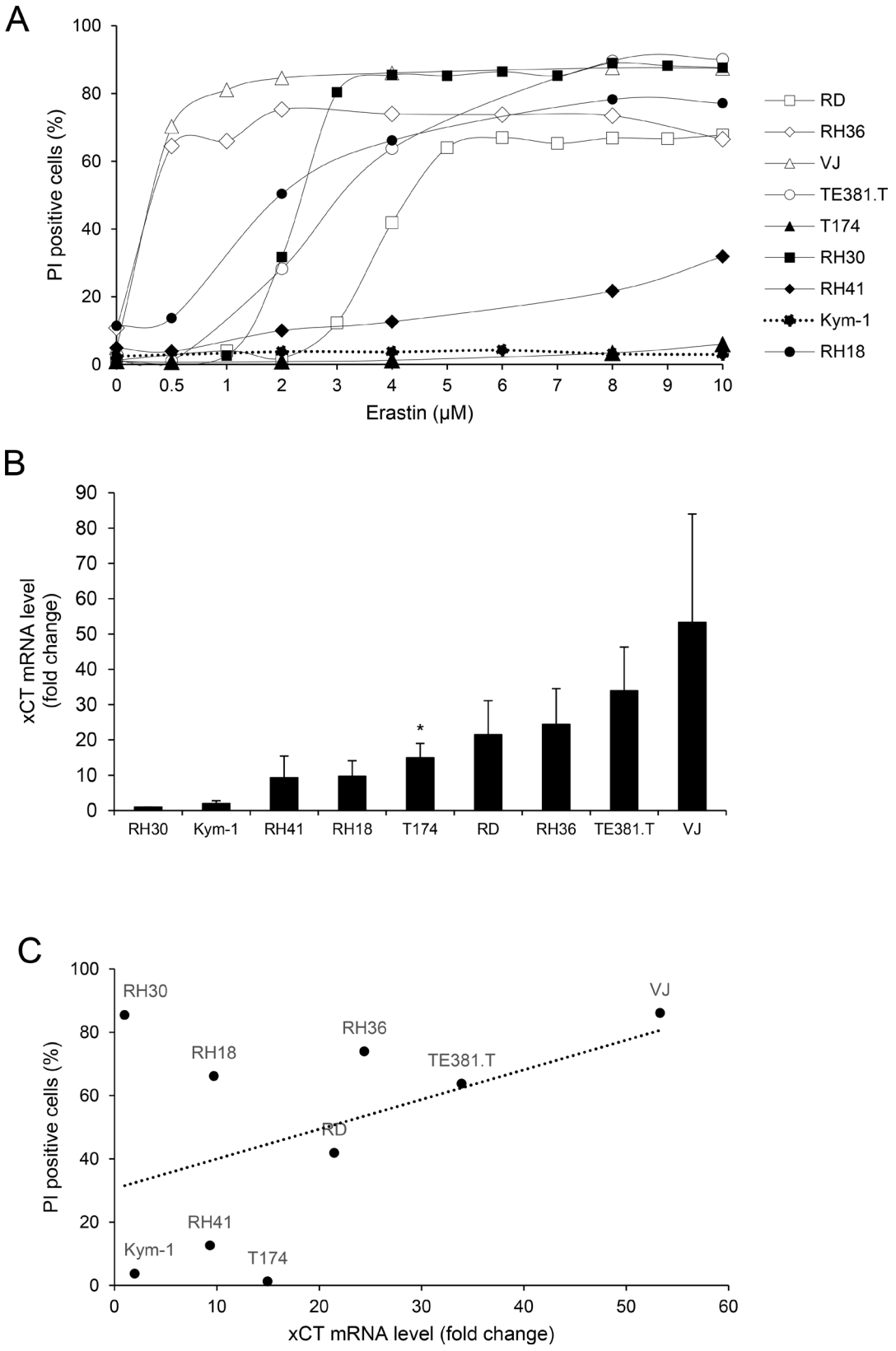

Figure 1: Erastin induces cell death in several RMS cell lines. RMS cells were treated with indicated concentrations of Erastin for 24 hours. Cell death was determined by analysis of PI/Hoechst staining and ImageXpress Micro XLS system (**A**). mRNA expression levels of xCT were analyzed by RT-PCR (**B**). The correlation between sensitivity to Erastin-induced cell death at 4 μM and xCT expression was analyzed using Excel ($y = 0.9394x + 30.555$; $R^2 = 0.2076$) (**C**). Mean and SEM (B) of at least three experiments performed in triplicate are shown; $^*P < 0.05$.

significantly reduced Erastin-induced cell death in a dose-dependent manner (Figure 5D). Also, Gö6976 significantly attenuated lipid peroxidation upon Erastin treatment (Figure 5F), while it did not prevent ROS production (Figure 5E).

Next, we used a genetic approach to test the involvement of PKCα. To this end, we knocked down PKCα by two distinct siRNA sequences (Figure 6A). Importantly, siRNA-mediated knockdown of PKCα significantly reduced Erastin-induced cell death in RMS (Figure 6B). This set of experiments suggests that in particular PKCα is indeed involved in regulating Erastin-induced ferroptotic cell death in RMS.

NOX inhibitors prevent Erastin-induced cell death, ROS production and lipid peroxidation

Since different PKC isoforms have been shown to act as upstream regulators of NOX isoforms [27], we then explored whether NOX are involved in ferroptotic

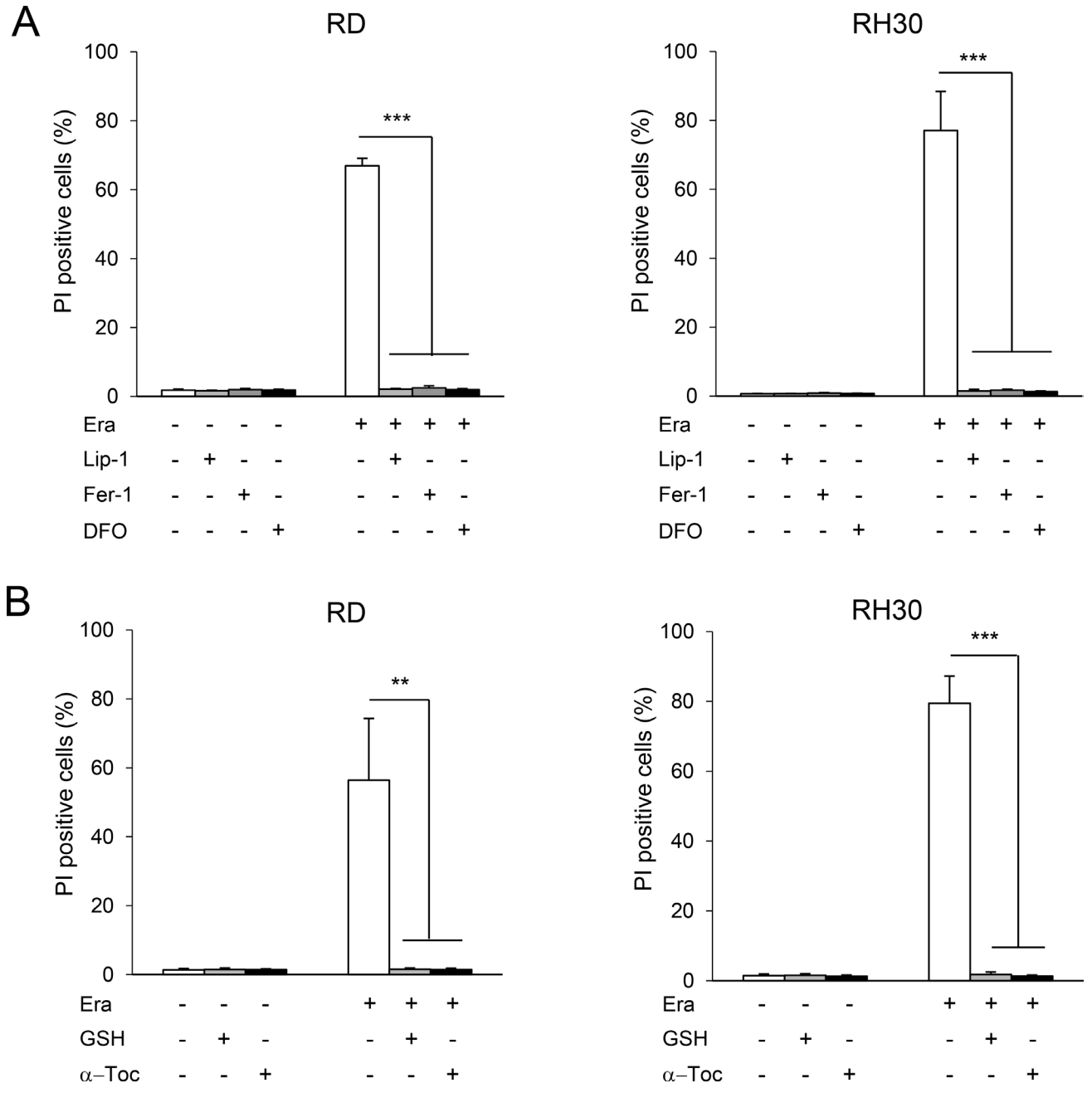

Figure 2: Erastin-induced cell death displays characteristic features of ferroptosis. RMS cells were treated with Erastin (RD: 5 μM; RH30: 3 μM) for 24 hours in the presence or absence of Lip-1 (50 nM), Fer-1 (5 μM), DFO (25 μM) (**A**), GSH (2.5 mM), α-Toc (100 μM) (**B**). Cell death was determined by analysis of PI/Hoechst staining and ImageXpress Micro XLS system. Mean and SD of at least three experiments performed in triplicate are shown; $^{**}P < 0.01$; $^{***}P < 0.001$.

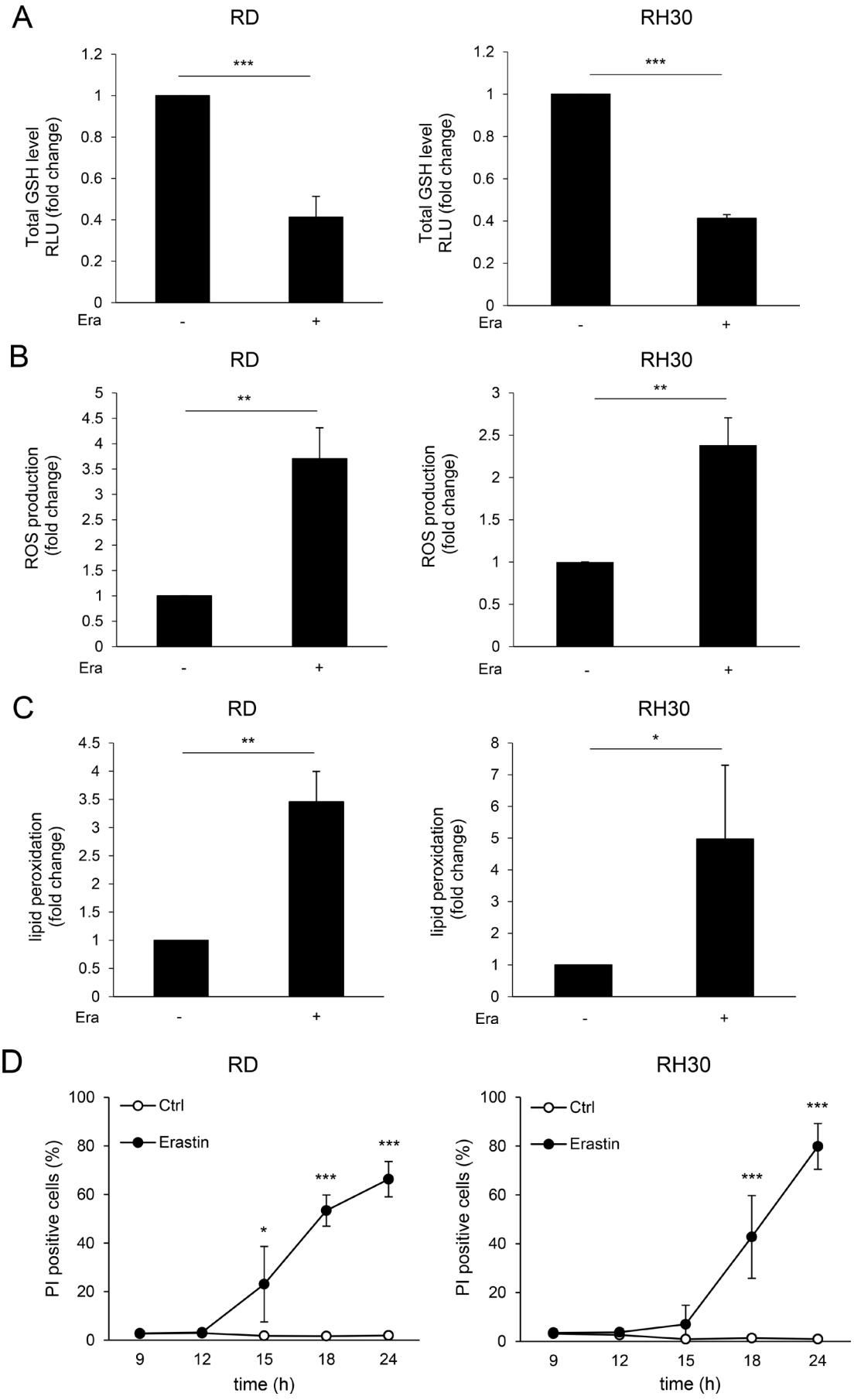
A
RD
RH30
Total GSH level
RLU (fold change)
***
Era
-
+
B
ROS production
(fold change)
**
C
lipid peroxidation
(fold change)
*
D
PI positive cells (%)
Ctrl
Erastin
time (h)

Figure 3: Erastin leads to GSH depletion, accompanied by ROS production and lipid peroxidation prior to cell death. GSH levels in RMS cells were determined after six hours of Erastin treatment (RD: 5 μM, RH30: 3 μM), using chemiluminescent GSH/GSSG-Glo Assay shown in relative light units (RLU) (**A**). ROS production (**B**) and lipid peroxidation (**C**) were determined after 12 hours of Erastin treatment using the fluorescent dyes H_2DCF (B) or BODIPY-C11 (C) and flow cytometry. RMS were treated with Erastin (RD: 5 μM, RH30: 3 μM) for indicated time points (**D**). Cell death was determined by analysis of PI/Hoechst staining and ImageXpress Micro XLS system. Mean and SD of at least three experiments performed in triplicate are shown; $^{*}P < 0.05$; $^{**}P < 0.01$; $^{***}P < 0.001$.

cell death. Intriguingly, addition of the broad-spectrum NOX inhibitor DPI significantly protected RMS cells from Erastin-induced cell death (Figure 7A). In addition, the NOX inhibitor GKT137831 that targets preferentially NOX1 and NOX4 [28] significantly reduced Erastin-triggered cell death (Figure 7B, Supplementary Figure

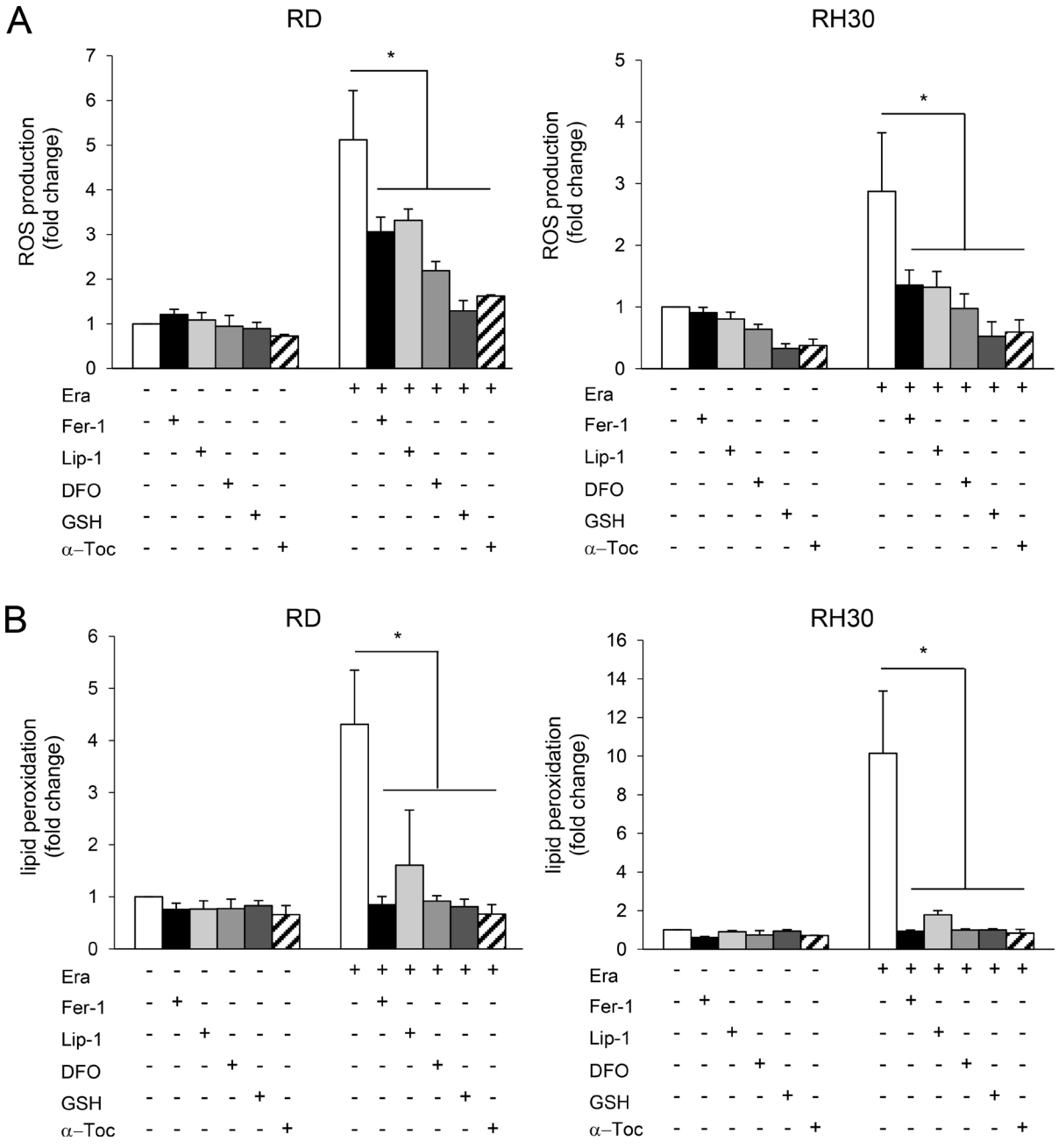

Figure 4: Erastin-induced ROS production and lipid peroxidation is decreased by ferroptosis inhibitors, ROS scavengers and DFO. RMS cells were treated with Erastin (RD: 5 μM; RH30: 3 μM) for 12 hours in the presence or absence of Fer-1 (5 μM), Lip-1 (50 nM), DFO (25 μM), GSH (2.5 mM) or α-Toc (100 μM). ROS production (**A**) and lipid peroxidation (**B**) were determined using the fluorescent dyes H_2DCF (A) or BODIPY-C11 and flow cytometry (B). Mean and SD of at least three experiments performed in triplicate are shown; $^{*}P < 0.05$.

4A). Consistently, Erastin-stimulated ROS production and lipid peroxidation were significantly decreased by DPI or GKT137831 (Figure 7C, 7D). To examine the role of NOX in other models of ferroptosis, we extended our analysis to RSL3. Notably, RSL3-induced ferroptosis was significantly reduced also in the presence of GKT137831 (Supplementary Figure 4B). These results suggest an involvement of NOX-dependent ROS production during Erastin-induced ferroptosis in RMS cells.

DISCUSSION

Since RMS have recently been reported to be vulnerable to oxidative stress [17], we tested in the present study whether RMS respond to Erastin, a compound described to stimulate oxidative stress-induced cell death [8]. Here, we report that RMS undergo ferroptosis upon treatment with Erastin. This conclusion is supported by

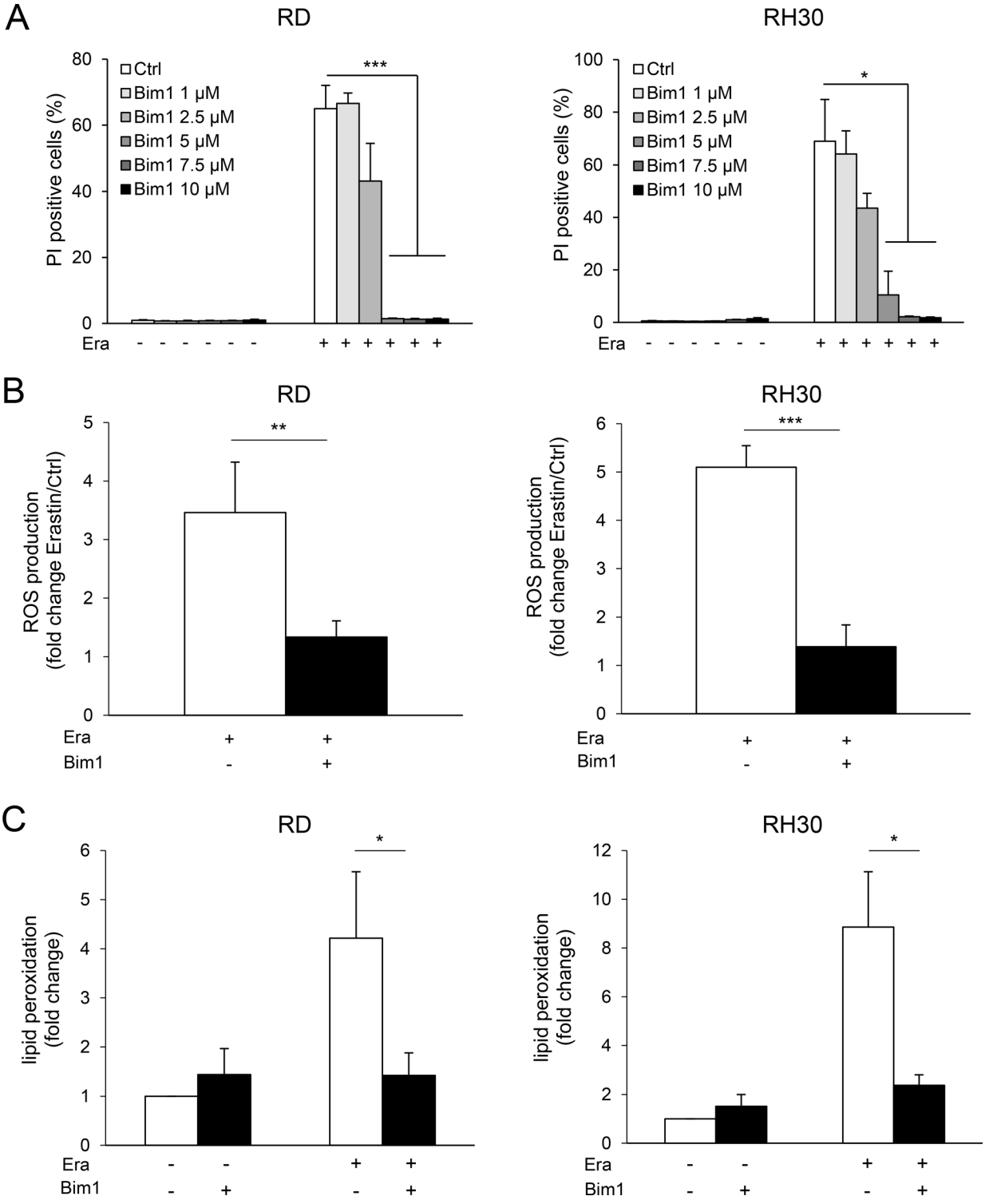

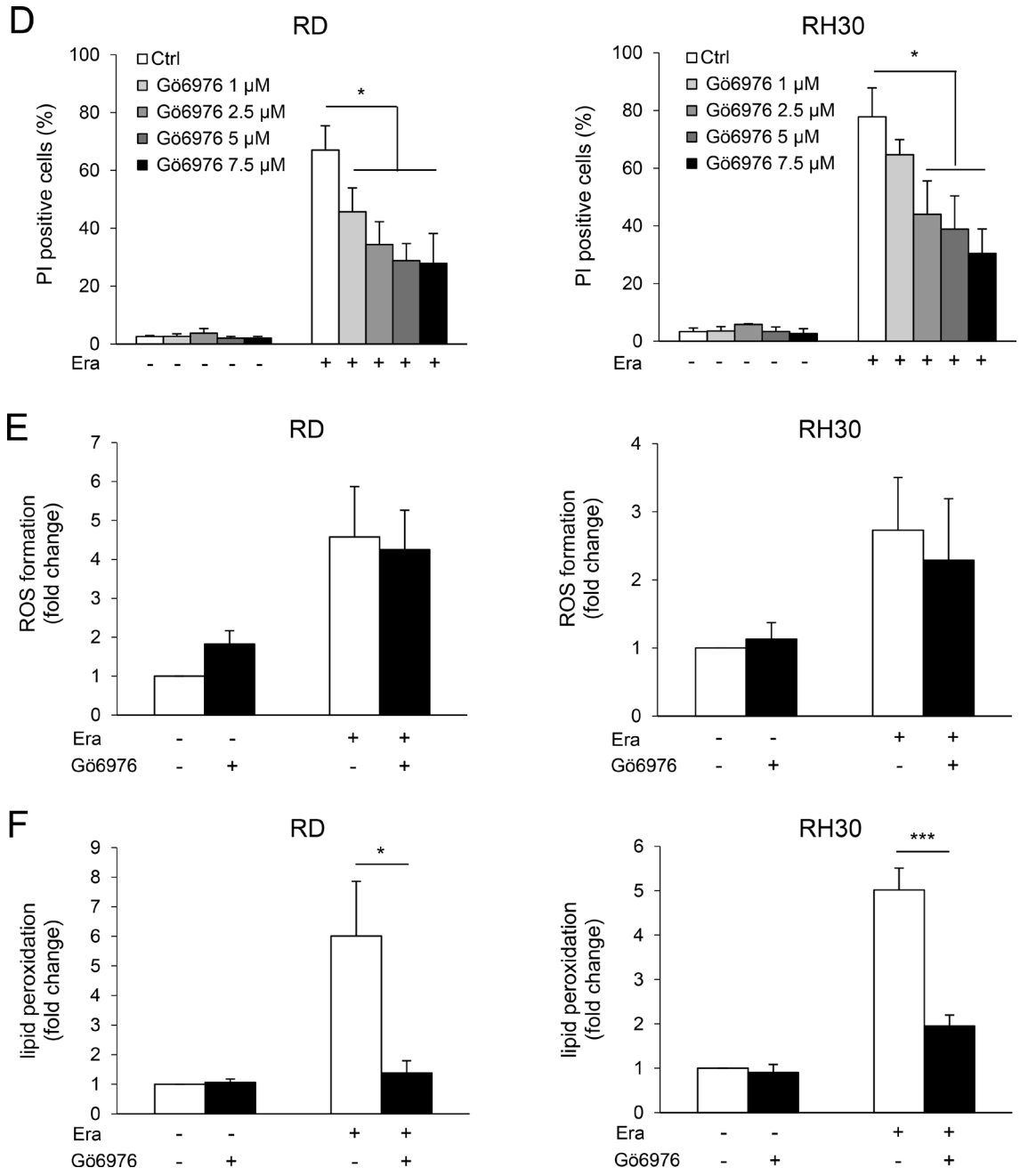

Figure 5: Pharmacological PKC inhibition blocks Erastin-induced cell death and lipid peroxidation. RMS cells were treated with Erastin (RD: 5 µM; RH30: 3 µM) for 24 hours in the presence or absence of the broad-spectrum PKC inhibitor Bim1 (**A**) or the PKCα and -β isoform-selective inhibitor Gö6976 (**D**) at indicated concentrations. Cell death was determined by analysis of PI/Hoechst staining and ImageXpress Micro XLS system (A, D). ROS production (**B**, **E**) and lipid peroxidation (**C**, **F**) were determined after 12 hours of Erastin treatment using the fluorescent dyes H_2DCF (B, E) or BODIPY-C11 (C, F) and flow cytometry. Because of the autofluorescence of Bim1, ROS production (B) is indicated as Erastin-treated cells normalized to control cells. Mean and SD of at least three experiments performed in triplicate are shown; $^{*}P < 0.05$; $^{**}P < 0.01$; $^{***}P < 0.001$.

our data showing that Erastin induced-cell death was associated with characteristic features of ferroptotic cell death such as lipid peroxidation, iron dependency and ROS production. Consistently, inhibitors of lipid peroxidation, ROS scavengers and an iron chelator all significantly rescued RMS from Erastin mediated-cell death. Sensitivity of the panel of tested RMS cell lines to Erastin did not significantly correlate with expression levels of xCT, known as a pharmacological target of Erastin [8, 19]. While a correlation between xCT expression levels and sensitivity to Erastin has been described [8], several additional factors are known to regulate ferroptosis, for example genes and proteins involved in iron or lipid metabolism [10].

Furthermore, we provided new insights into the molecular mechanisms of ferroptosis. We showed that PKC and in particular PKCα were involved as mediators of Erastin-induced cell death. This notion is supported by our findings showing that not only the broad-spectrum PKC inhibitor Bim1, but also the PKCα/β-selective inhibitor Gö6976 protected RMS cells from Erastin-generated lipid peroxidation and cell death. In addition, genetic silencing of PKCα protected RMS cells from Erastin-induced cell death emphasizing the involvement of PKCα in ferroptotic signaling. Interestingly, PKCα has recently been described to initiate ferroptotic cell death in dopaminergic neurons in a model of Parkinson's disease [24].

Besides PKC, our study points to an involvement of NOX in ROS signaling and ferroptotic cell death in RMS, since the broad-spectrum NOX inhibitor DPI as well as the selective NOX1/4 inhibitor GKT137831 rescued RMS cells from Erastin-stimulated ROS production, lipid peroxidation and cell death. Ferroptosis is an iron-dependent, oxidative form of cell death, and several ROS-producing enzymes, including NOX, require iron for their proper function [16]. NOX are activated via various mechanisms, including phosphorylation, by PKC and other kinases [29–31], oxidative stress [32] and arachidonic acid [33], which all have been implicated in ferroptotic signaling [9]. Thus, NOX might be involved in ferroptosis as a source of ROS production. Indeed, NOX have been implicated in ferroptotic signaling in non-small lung cancer cells, since the addition of DPI and GKT137831 inhibited Erastin-stimulated cell death [8].

Our study has implications for therapeutic targeting of the redox balance in RMS. We identify in the present study the vulnerability of RMS cells to ferroptosis as a prototypic form of oxidative, iron-dependent cell death. While targeting GSH homeostasis by agents like sorafenib, buthionine sulphoximine (BSO) and oxidative stress-inducing compounds like auranofin, carfilzomib and cerivastatin has previously been reported as a possible therapeutic strategy for RMS *in vitro* and *in vivo* [17, 34, 35], Erastin has not yet been tested in RMS in

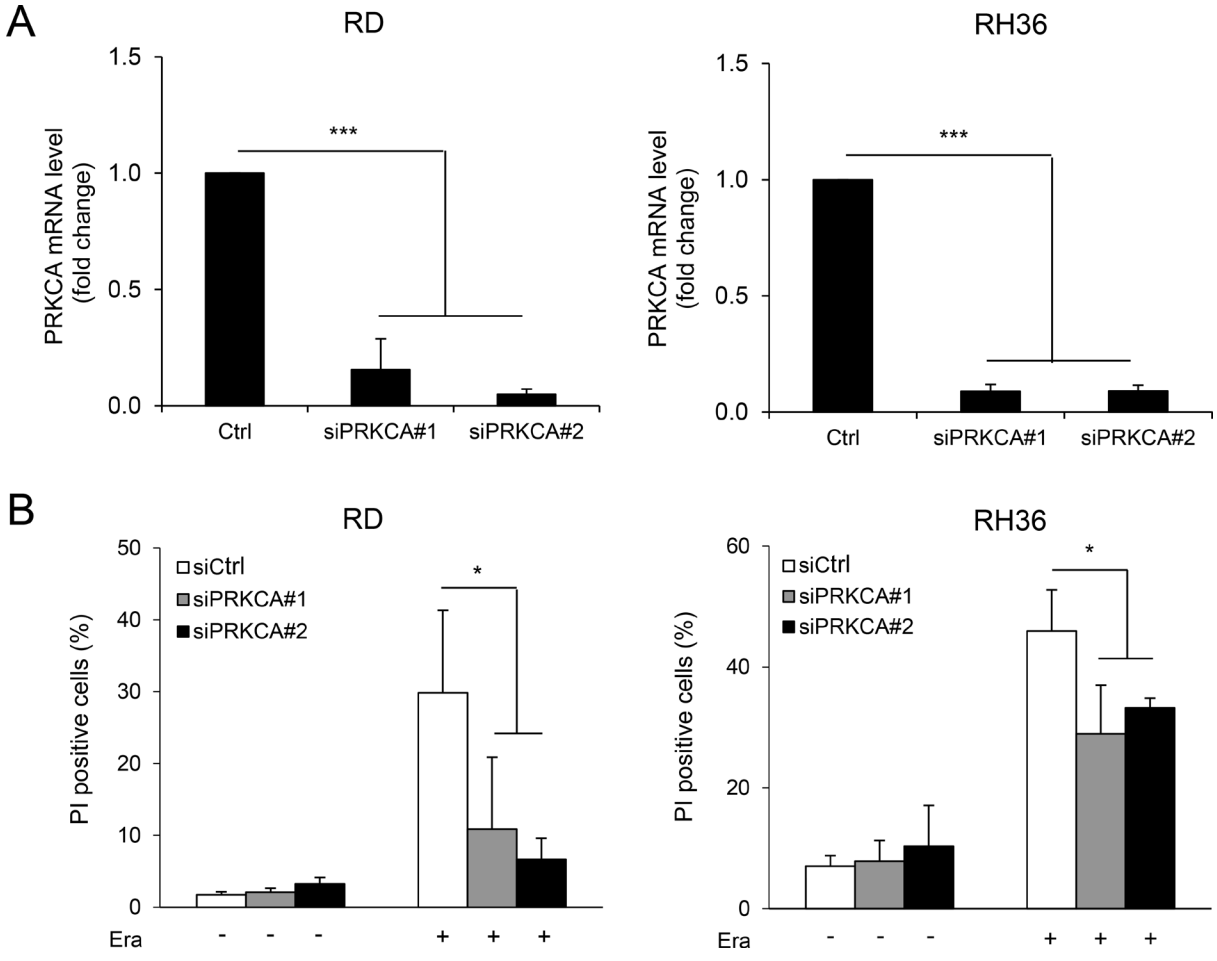

Figure 6: siRNA-mediated knockdown of PKCα rescues from Erastin-induced cell death. RMS cells (RD, RH36) were transiently transfected with siRNAs against PKCα or control siRNA. mRNA levels of PKCα were analyzed by qRT-PCR (**A**). RMS were treated with Erastin (RD 5 μM; RH36 2 μM) for 15 hours (RD) or 22 hours (RH36) and cell death was determined by PI/Hoechst staining and ImageXpress Micro XLS system (**B**). Mean and SD of at least three experiments performed in triplicate are shown; $^{*}P < 0.05$; $^{***}P < 0.001$.

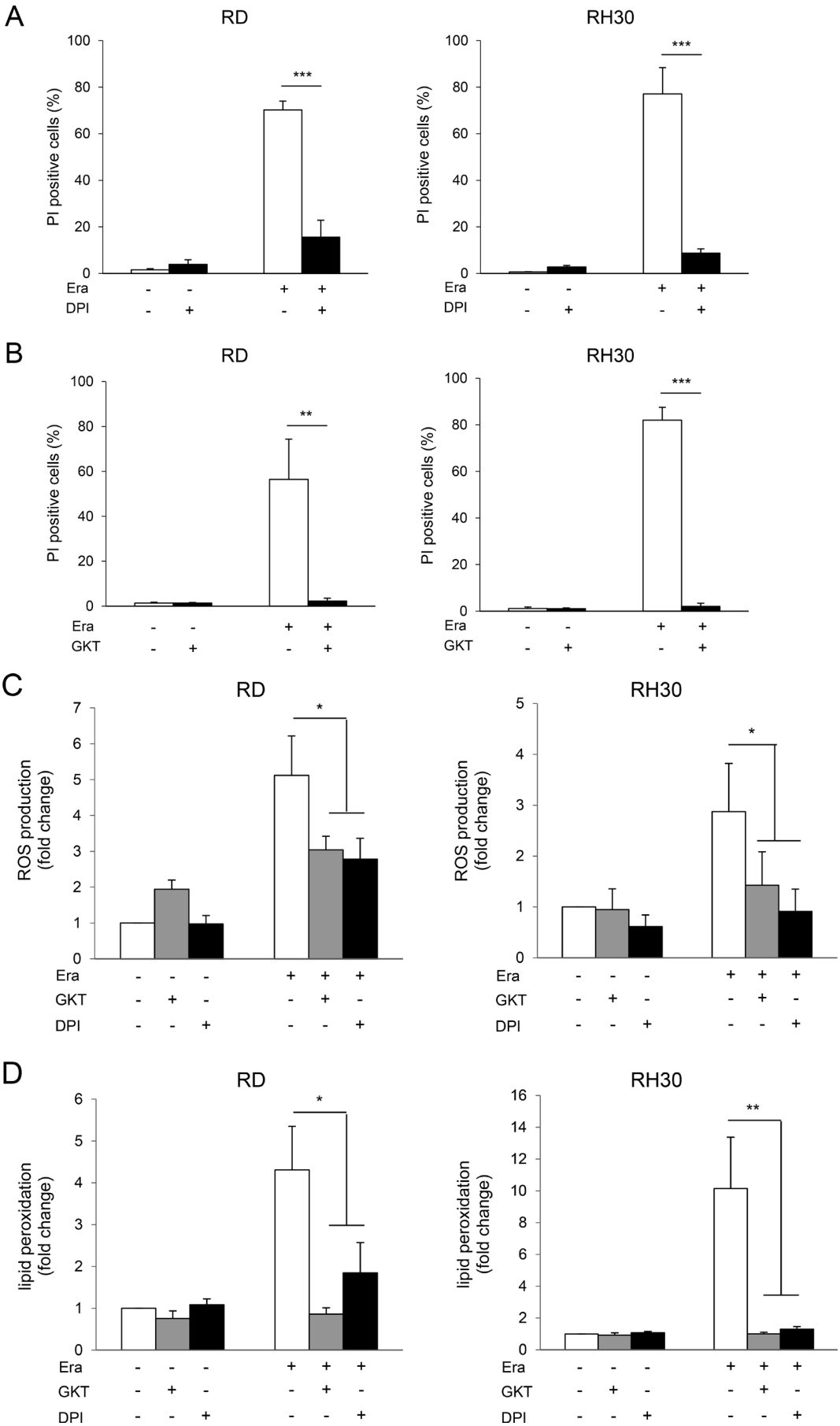
A
RD
RH30
PI positive cells (%)
***
Era
DPI
B
RD
RH30
PI positive cells (%)
**
***
Era
GKT
C
RD
RH30
ROS production (fold change)
*
Era
GKT
DPI
D
RD
RH30
lipid peroxidation (fold change)
*
**
Era
GKT
DPI

Figure 7: NOX inhibitors prevent Erastin-induced cell death, ROS production and lipid peroxidation. RMS cells were treated with Erastin (RD: 5 μM; RH30: 3 μM) for 24 hours in the presence or absence of DPI (1 μM) (**A**) or GKT137831 (20 μM) (**B**). Cell death was determined by PI/Hoechst staining and ImageXpress Micro XLS system (A, B). ROS production (**C**) and lipid peroxidation (**D**) were determined by the fluorescent dyes H_2DCF (C) or BODIPY-C11 (D) and flow cytometry. Mean and SD of at least three experiments performed in triplicate are shown; $^{*}P < 0.05$; $^{**}P < 0.01$; $^{***}P < 0.001$.

contrast to many other cancer types [20]. An analogue of Erastin (i.e. PRLX 93936) is currently being evaluated in phase 1/2 clinical trials in patients with multiple myeloma (ClinicalTrials.gov identifier: NCT01695590), emphasizing the relevance of Erastin-derived analogues as new cancer therapeutics. Thus, ferroptosis might provide new perspectives to reactivate programmed cell death in RMS, especially in refractory or relapsed disease, where therapeutic options are limited.

MATERIALS AND METHODS

Cell culture and chemicals

Human RMS cell lines were obtained from American Type Culture Collection (Manassas, VA, USA) or from the Deutsche Sammlung von Mikroorganismen und Zellkulturen GmbH (Braunschweig, Germany) and cultured in RPMI 1640 or Dulbecco's Modified Eagle Medium (DMEM) (Life Technologies, Inc., Eggenstein, Germany), supplemented with 10% fetal calf serum (FCS) (Biochrom, Berlin, Germany), 1 mM glutamine (Invitrogen, Karlsruhe, Germany), 1% penicillin/streptomycin (Invitrogen) and 25 mM HEPES (Biochrom). Primary cultured RMS cells were generated from a tumor sample derived from a patient diagnosed with fusion gene-negative eRMS. All cell lines were authenticated by STR profiling and continuously monitored for mycoplasma contamination. Erastin, Lip-1, DFO, Fer-1, α-Toc, NAC and DPI were obtained from Sigma-Aldrich (Steinheim, Germany), reduced GSH by Carl Roth (Karlsruhe, Germany). GKT137831 was purchased from Selleck Chemicals (Houston, USA), whereas Bim1 was obtained from Cayman Chemicals (Michigan, USA) and Gö6976 from Tocris Bioscience (Bristol, UK). RSL3 was purchased from InterBIOScreen Ltd. (Moscow, Russia). All chemicals were purchased from Sigma-Aldrich or Carl Roth unless indicated otherwise.

Determination of cell death, intracellular GSH levels, ROS production and lipid peroxidation

Cell death was assessed by Hoechst/propidium iodide (PI) staining, analyzing the plasma membrane permeability using fluorescence microscopy (ImageXpress Mikro XLS), as described previously [36]. To determine cellular GSH levels, GSH/GSSG-Glo assay (Promega, Madison, WI, USA) was used following the instruction manual. In parallel, cells were stained with 1 μg/μl Hoechst-Dye (Sigma-Aldrich) and measured by fluorescence microscopy (ImageXpress Mikro XLS) with automated analysis using MetaXpress Software (Molecular Devices).

ROS production and lipid peroxidation were analyzed at early time points before cells succumb to cell death to monitor events prior to the induction of cell death as previously described [37]. To analyze ROS production cells were pelleted and resuspended with phenol-free medium (RPMI) containing 5 μM of the fluorescent dye CM-H_2DCFDA (Invitrogen), which has been reported to detect ROS such as hydrogen peroxides, hydroxyl radicals or peroxyl radicals, for 30 minutes at 37° C and immediately analyzed by flow cytometry using FITC channel. For determination of lipid peroxidation cells were pelleted and resuspended with PBS containing 5 μM of the fluorescent dye BODIPY-C11 (Invitrogen) for 30 minutes at 37° C and immediately analyzed by flow cytometry using FITC channel.

Transient transfection

For transient knockdown by siRNA, cells were reversely transfected with 10 nM SilencerSelect siRNA (Life Technologies, Inc.), that is, control siRNA (4390842 siCtrl) or targeting siRNA for PRKCA (s11092 siPKRCA#1, s11094 siPKRCA#2) using lipofectamine RNAiMAX. Briefly, 1.5 μl lipofectamine or 10 nM siRNA were diluted in 25 μl Opti-MEM, mixed, incubated for 10 minutes and transferred into a 24-well plate. Cells were then seeded onto the transfection mixture.

RT-PCR

xCT and PKC mRNA levels were determined by quantitative real-time PCR (qRT-PCR) analysis, as previously described [38]. Total RNA extraction and cDNA synthesis were performed following the instruction manual, xCT and PKC levels were assessed by SYBR®Green Expression Assay purchased from Eurofins Genomics (Ebersberg, Germany) and GAPDH levels by SYBR®Green qPCR assay from Applied Biosystems (Darmstadt, Germany) according to the manufacturer's instructions using the Quantstudio 7 Flex real-time PCR system from Applied Biosystems. The following primers were used (sequence 5′->3′). xCT (forward primer: CCTCTATTCGGACCCATTTAGT, reverse primer: CTGGGTTTCTTGTCCCATAA), PKCα (forward primer: TCGACTGGGAAAAACTGGAG, reverse primer: CTCTGCTCCTTTGCCACAC), PKCβ (forward primer: CTTCAAGCAGCCCACCTTCT, reverse primer: TCCCCGAAGCCCCAGATG), PKCδ (forward primer: ATTATCCCCGCTGGATCAC, reverse primer:

CTTGGTTGGTTCCCTTTCAA), PKCε (forward primer: AACACCCGTACCTTACCCAAC, reverse primer: CGAAAAAGAGGCGGTCCT). Relative expression of target gene transcript and reference gene transcript was calculated as ΔΔCt. GAPDH was used as reference gene.

Statistical analysis

Statistical significance was assessed using Student's *t*-Test (two-tailed distribution, equal variance) calculated with Microsoft Excel (Munich, Germany).

ACKNOWLEDGMENTS

We thank C. Hugenberg for expert secretarial assistance.

CONFLICTS OF INTEREST

The authors declare that they do not have any conflicts of interest.

FUNDING

This work has been partially supported by grants from the BMBF (to S.F.).

REFERENCES

1. Kramer S, Meadows AT, Jarrett P, Evans AE. Incidence of childhood cancer: experience of a decade in a population-based registry. J Natl Cancer Inst. 1983; 70:49–55.
2. Egas-Bejar D, Huh WW. Rhabdomyosarcoma in adolescent and young adult patients: current perspectives. Adolesc Health Med Ther. 2014; 5:115–125.
3. Hayes-Jordan A, Andrassy R. Rhabdomyosarcoma in children. Curr Opin Pediatr. 2009; 21:373–378.
4. Hinson AR, Jones R, Crose LE, Belyea BC, Barr FG, Linardic CM. Human rhabdomyosarcoma cell lines for rhabdomyosarcoma research: utility and pitfalls. Front Oncol. 2013; 3:183.
5. Hengartner MO. The biochemistry of apoptosis. Nature. 2000; 407:770.
6. Berghe TV, Linkermann A, Jouan-Lanhouet S, Walczak H, Vandenabeele P. Regulated necrosis: the expanding network of non-apoptotic cell death pathways. Nat Rev Mol Cell Biol. 2014; 15:135–147.
7. Conrad M, Angeli JP, Vandenabeele P, Stockwell BR. Regulated necrosis: disease relevance and therapeutic opportunities. Nat Rev Drug Discov. 2016; 15:348–366.
8. Dixon SJ, Lemberg KM, Lamprecht MR, Skouta R, Zaitsev EM, Gleason CE, Patel DN, Bauer AJ, Cantley AM, Yang WS, Morrison B, Stockwell BR. Ferroptosis: An Iron-Dependent Form of Nonapoptotic Cell Death. Cell. 2012; 149:1060–1072.
9. Kagan VE, Mao G, Qu F, Angeli JP, Doll S, Croix CS, Dar HH, Liu B, Tyurin VA, Ritov VB, Kapralov AA, Amoscato AA, Jiang J, et al. Oxidized arachidonic and adrenic PEs navigate cells to ferroptosis. Nat Chem Biol. 2017; 13:81–90.
10. Cao JY, Dixon SJ. Mechanisms of ferroptosis. Cell Mol Life Sci. 2016; 73:2195–2209.
11. Yu H, Guo P, Xie X, Wang Y, Chen G. Ferroptosis, a new form of cell death, and its relationships with tumourous diseases. J Cell Mol Med. 2017; 21:648–657.
12. Dolma S, Lessnick SL, Hahn WC, Stockwell BR. Identification of genotype-selective antitumor agents using synthetic lethal chemical screening in engineered human tumor cells. Cancer Cell. 2003; 3:285–296.
13. Yang WS, Stockwell BR. Synthetic lethal screening identifies compounds activating iron-dependent, nonapoptotic cell death in oncogenic-RAS-harboring cancer cells. Chem Biol. 2008; 15:234–45.
14. Yang Wan S, SriRamaratnam R, Welsch Matthew E, Shimada K, Skouta R, Viswanathan Vasanthi S, Cheah Jaime H, Clemons Paul A, Shamji Alykhan F, Clish Clary B, Brown Lewis M, Girotti Albert W, Cornish Virginia W, et al. Regulation of Ferroptotic Cancer Cell Death by GPX4. Cell. 2014; 156:317–331.
15. Stockwell BR, Friedmann Angeli JP, Bayir H, Bush AI, Conrad M, Dixon SJ, Fulda S, Gascon S, Hatzios SK, Kagan VE, Noel K, Jiang X, Linkermann A, et al. Ferroptosis: A Regulated Cell Death Nexus Linking Metabolism, Redox Biology, and Disease. Cell. 2017; 171:273–285.
16. Dixon SJ, Stockwell BR. The role of iron and reactive oxygen species in cell death. Nat Chem Biol. 2014; 10:9–17.
17. Chen X, Stewart E, Shelat AA, Qu C, Bahrami A, Hatley M, Wu G, Bradley C, McEvoy J, Pappo A, Spunt S, Valentine MB, Valentine V, et al. Targeting oxidative stress in embryonal rhabdomyosarcoma. Cancer Cell. 2013; 24:710–724.
18. Fan TWM, Kucia M, Jankowski K, Higashi RM, Ratajczak J, Ratajczak MZ, Lane AN, Jankowski K, Kucia M, Wysoczynski M, Reca R, Zhao D, Trzyna E, et al. Rhabdomyosarcoma cells show an energy producing anabolic metabolic phenotype compared with primary myocytes. Mol Cancer. 2008; 7:79–79.
19. Sato M, Kusumi R, Hamashima S, Kobayashi S, Sasaki S, Komiyama Y, Izumikawa T, Conrad M, Bannai S, Sato H. The ferroptosis inducer erastin irreversibly inhibits system xc- and synergizes with cisplatin to increase cisplatin's cytotoxicity in cancer cells. Sci Rep. 2018; 8:968.
20. Xie Y, Hou W, Song X, Yu Y, Huang J, Sun X, Kang R, Tang D. Ferroptosis: process and function. Cell Death Differ. 2016; 23:369–379.
21. Skouta R, Dixon SJ, Wang J, Dunn DE, Orman M, Shimada K, Rosenberg PA, Lo DC, Weinberg JM, Linkermann A, Stockwell BR. Ferrostatins inhibit oxidative lipid damage

and cell death in diverse disease models. Journal of the American Chemical Society. 2014; 136:4551–4556.

22. Friedmann Angeli JP, Schneider M, Proneth B, Tyurina YY, Tyurin VA, Hammond VJ, Herbach N, Aichler M, Walch A, Eggenhofer E, Basavarajappa D, Rådmark O, Kobayashi S, et al. Inactivation of the ferroptosis regulator Gpx4 triggers acute renal failure in mice. Nat Cell Biol. 2014; 3:1–9.
23. Yant LJ, Ran Q, Rao L, Van Remmen H, Shibatani T, Belter JG, Motta L, Richardson A, Prolla TA. The selenoprotein GPX4 is essential for mouse development and protects from radiation and oxidative damage insults. Free Radic Biol Med. 2003; 34:496–502.
24. Do Van B, Gouel F, Jonneaux A, Timmerman K, Gele P, Petrault M, Bastide M, Laloux C, Moreau C, Bordet R, Devos D, Devedjian JC. Ferroptosis, a newly characterized form of cell death in Parkinson's disease that is regulated by PKC. Neurobiol Dis. 2016; 94:169–178.
25. Komander D, Kular GS, Schuttelkopf AW, Deak M, Prakash KR, Bain J, Elliott M, Garrido-Franco M, Kozikowski AP, Alessi DR, van Aalten DM. Interactions of LY333531 and other bisindolyl maleimide inhibitors with PDK1. Structure. 2004; 12:215–226.
26. Martiny-Baron G, Kazanietz MG, Mischak H, Blumberg PM, Kochs G, Hug H, Marme D, Schachtele C. Selective inhibition of protein kinase C isozymes by the indolocarbazole Go 6976. J Biol Chem. 1993; 268:9194–9197.
27. Cosentino-Gomes D, Rocco-Machado N, Meyer-Fernandes JR. Cell signaling through protein kinase C oxidation and activation. Int J Mol Sci. 2012; 13:10697–10721.
28. Aoyama T, Paik YH, Watanabe S, Laleu B, Gaggini F, Fioraso-Cartier L, Molango S, Heitz F, Merlot C, Szyndralewiez C, Page P, Brenner DA. Nicotinamide adenine dinucleotide phosphate oxidase in experimental liver fibrosis: GKT137831 as a novel potential therapeutic agent. Hepatology. 2012; 56:2316–2327.
29. Rastogi R, Geng X, Li F, Ding Y. NOX Activation by Subunit Interaction and Underlying Mechanisms in Disease. Front Cell Neurosci. 2016; 10:301.
30. Lewis EM, Sergeant S, Ledford B, Stull N, Dinauer MC, McPhail LC. Phosphorylation of p22phox on threonine 147 enhances NADPH oxidase activity by promoting p47phox binding. J Biol Chem. 2010; 285:2959–2967.
31. Brandes RP, Weissmann N, Schroder K. Nox family NADPH oxidases: Molecular mechanisms of activation. Free Radic Biol Med. 2014; 76:208–226.
32. Li WG, Miller FJ Jr, Zhang HJ, Spitz DR, Oberley LW, Weintraub NL. H(2)O(2)-induced O(2) production by a non-phagocytic NAD(P)H oxidase causes oxidant injury. J Biol Chem. 2001; 276:29251–29256.
33. Colston JT, de la Rosa SD, Strader JR, Anderson MA, Freeman GL. H2O2 activates Nox4 through PLA2-dependent arachidonic acid production in adult cardiac fibroblasts. FEBS Lett. 2005; 579:2533–2540.
34. Maruwge W, D'Arcy P, Folin A, Brnjic S, Wejde J, Davis A, Erlandsson F, Bergh J, Brodin B. Sorafenib inhibits tumor growth and vascularization of rhabdomyosarcoma cells by blocking IGF-1R-mediated signaling. Onco Targets Ther. 2008; 1:67–78.
35. Castro B, Alonso-Varona A, del Olmo M, Bilbao P, Palomares T. Role of gamma-glutamyltranspeptidase on the response of poorly and moderately differentiated rhabdomyosarcoma cell lines to buthionine sulfoximine-induced inhibition of glutathione synthesis. Anticancer Drugs. 2002; 13:281–291.
36. Haydn T, Metzger E, Schuele R, Fulda S. Concomitant epigenetic targeting of LSD1 and HDAC synergistically induces mitochondrial apoptosis in rhabdomyosarcoma cells. Cell Death Dis. 2017; 8:e2879.
37. Habermann KJ, Grunewald L, van Wijk S, Fulda S. Targeting redox homeostasis in rhabdomyosarcoma cells: GSH-depleting agents enhance auranofin-induced cell death. Cell Death Dis. 2017; 8:e3067.
38. Heinicke U, Kupka J, Fichter I, Fulda S. Critical role of mitochondria-mediated apoptosis for JNJ-26481585-induced antitumor activity in rhabdomyosarcoma. Oncogene. 2016; 35:3729–3741.